Eur Biophys J (2011) 40:1131–1142
DOI 10.1007/s00249-011-0744-x

ORIGINAL PAPER

Biophysical studies of an NAD(P)$^+$-dependent aldehyde dehydrogenase from *Bacillus licheniformis*

Huei-Fen Lo · Jian-Yu Su · Hsiang-Ling Chen · Jui-Chang Chen · Long-Liu Lin

Received: 16 May 2011 / Accepted: 9 August 2011 / Published online: 27 August 2011

Abstract Aldehyde dehydrogenase (ALDH) catalyzes the conversion of aldehydes to the corresponding acids by means of an NAD(P)$^+$-dependent virtually irreversible reaction. In this investigation, the biophysical properties of a recombinant *Bacillus licheniformis* ALDH (*Bl*ALDH) were characterized in detail by analytical ultracentrifuge (AUC) and various spectroscopic techniques. The oligomeric state of *Bl*ALDH in solution was determined to be tetrameric by AUC. Far-UV circular dichroism analysis revealed that the secondary structures of *Bl*ALDH were not altered in the presence of acetone and ethanol, whereas SDS had a detrimental effect on the folding of the enzyme. Thermal unfolding of this enzyme was found to be highly irreversible. The native enzyme started to unfold beyond ~0.2 M guanidine hydrochloride (GdnHCl) and reached an unfolded intermediate, $[GdnHCl]_{05,\ N\text{-}U}$, at 0.93 M. *Bl*ALDH was active at concentrations of urea below 2 M, but it experienced an irreversible unfolding under 8 M denaturant. Taken together, this study provides a foundation for the future structural investigation of *Bl*ALDH, a typical member of ALDH superfamily enzymes.

Keywords Aldehyde dehydrogenase · *Bacillus licheniformis* · Oligomeric state · Analytical ultracentrifuge · Circular dichroism · Fluorescence spectroscopy

Huei-Fen Lo and Jian-Yu Su contributed equally to this work.

H.-F. Lo · H.-L. Chen
Department of Food Science and Technology, Hungkuang University, 34 Chungchie Road, Shalu, Taichung City, Taiwan

J.-Y. Su · J.-C. Chen · L.-L. Lin (✉)
Department of Applied Chemistry, National Chiayi University, 300 Syuefu Road, Chiayi City 60004, Taiwan
e-mail: llin@mail.ncyu.edu.tw

Introduction

Aldehyde dehydrogenases (ALDHs; EC 1.2.1.3) belong to the short-chain dehydrogenases/reductases (SDRs) superfamily, which is characterized by a Gly-motif in the coenzyme-binding regions and a catalytic tetrad (Persson et al. 2009), and they catalyze the oxidation (dehydrogenation) of aldehydes to the corresponding acids. Aldehydes are cytotoxic and mutagenic compounds that are present in the environment as a result of industrial activity (Vasiliou et al. 2000), although they can also be formed endogenously during the metabolism of amino acids, vitamins, lipids, and carbohydrates (Sripo et al. 2002). Since ALDH activity plays an important role as the detoxifying agent to overcome the harmful effects of these compounds, a vast number of ALDHs have been studied extensively (Sophos and Vasiliou 2003; Vasiliou and Nebert 2005; Parés et al. 2008). Based on the sequences, the enzymes are classified into different classes (Vasiliou et al. 1995; Yoshida et al. 1998), including phenylacetaldehyde dehydrogenase, lactaldehyde dehydrogenase, bacterial ALDH, human ALDH, and yeast ALDH. Though many of these enzymes have been characterized with respect to substrate specificity, perhaps the best-studied ones are the mammalian ALDHs from liver cytosol (Hart and Dickinson 1982; Vallari and Pietruszko 1984; Dickinson and Haywood 1986), liver mitochondria (Feldman and Weiner 1972; Sidhu and Blair 1975; Zheng et al. 1993; Ni et al. 1997; Sheikh et al. 1997), and stomach cytosol (Hsu et al. 1992; Mann and Weiner 1999; Hempel et al. 2001), and the bacterial ALDHs from *Escherichia coli* (Ho and Weiner 2005), *Vibrio cholerae* (Parsot and Mekalanos 1991), and *Alcaligenes eutrophus* (Priefert et al. 1992).

All ALDHs that have been characterized in the SDR superfamily are homobiopolymers composed of two or four

polypeptides of 50–55 kDa (Perozich et al. 1999). To date, several crystal structures of the ALDH enzyme have been determined, starting with *Rattus norvegicus* ALDH3 (Liu et al. 1997) and extending to *Bos taurus* ALDH2 (Steinmetz et al. 1997), *Gadus callarias* ALDH9 (Johansson et al. 1998), *Ovis aries* ALDH1 (Moore et al. 1998), *Mus musculus* ALDH (Lamb and Newcomer 1999), and *Streptococcus mutans* ALDH (Cobessi et al. 1999). According to the determined structures, the ALDH monomer comprises an N-terminal cofactor (NAD/P^+)-binding domain, a catalytic domain, and an oligomerization domain. The cofactor-binding domain can be further divided into a core element resembling a Rossmann fold with an $\alpha\beta_5$ structure surrounded by substructures of antiparallel β-strands (β1–4) and α-helices (α1–5). The catalytic domain adopts an α/β topology formed by six parallel twisted β-strands and an antiparallel β-strand (β14) connected by six helices. The oligomerization domain comprises two antiparallel twisted β-strands (β6 and β21) and helix α21, and docks into a groove formed at the interface between the catalytic domain and the cofactor-binding domain of the second monomer. Sequence comparison shows that the active site is largely conserved throughout the different classes of the ALDH enzyme and the overall conformation of this site changes very little (Perez-Miller and Hurley 2003). The central feature of the active site of the ALDH enzyme is a Cys nucleophile, which forms a thiohemiacetal derivative with the aldehyde before transfer of a hybride to $NAD(P)^+$ to form an acylated intermediate that is hydrolyzed to the corresponding acid. Three polar conserved residues in the active site of the crystallized ALDHs are an asparagine proposed to stabilize the thiohemiacetal derivative (Hurley et al. 1999; Hempel et al. 1999) and two glutamates situated in the vicinity of the Cys nucleophile. Depending on the specific ALDH, one or the other of the Glu residues has been implicated to function as a general base and assist in the deprotonation of the Cys nucleophile (Hempel et al. 1999; Wang and Weiner 1995). However, due to the large distance from the Cys nucleophile, the Glu residue must mediate its effect via a water molecule or another polar residue and/or be brought in proximity to the Cys nucleophile by a conformational change (Marchal et al. 2001).

The participation of ALDHs in the metabolic pathway is widespread among living organisms. For instance, lactaldehyde and phenylacetaldehyde dehydrogenases of *Escherichia coli* K-12 participate in the degradation pathways of race carbon sources (Cabellero et al. 1983; Hanlon et al. 1997), a plant betainealdehyde dehydrogenase is involved in osmolarity regulation (Weretilnyk and Hanson 1990), a retialdehyde dehydrogenase is essential for cell development and differentiation (Niederreither et al. 2001), and *Euglena gracilis* ALDH plays a critical role in the energy metabolism of this protist (Rodríguez-Zavala et al. 2006).

In *Bacillus licheniformis*, more than 10 *ALDH* genes have been identified (Veith et al. 2004), and one of these genes, *ybcD*, encodes an ALDH of 488 amino acid residues that has recently been characterized (Lo and Chen 2010). Although *B. licheniformis* is used extensively for the commercial production of exoenzymes (Schallmey et al. 2004), bacitracins (Ming and Epperson 2002; Murphy et al. 2007), and various organic metabolites (Birrer et al. 1994; Zuo 2007), the biochemical and biophysical studies of industrially viable ALDHs of this bacterium are still largely obscure. In this study, we have focused on the biophysical characterization of *Bl*ALDH using analytical ultracentrifugation (AUC), circular dichroism (CD), and intrinsic tryptophan fluorescence measurements. Our results provide clues to the oligomeric state, the stability in different environmental conditions, and the chemical-induced unfolding of the enzyme.

Materials and methods

Materials

Luria-Bertani (LB) medium was acquired from Difco Laboratories (Detroit, MI, USA). Ampicillin, kanamycin, NAD^+, NADH, imidazole, guanidine hydrochloride, and urea were obtained from Sigma-Aldrich Fine Chemicals (St. Louis, MO, USA). Ni^{2+}-nitrilotriacetate (Ni^{2+}-NTA) resin was purchased from Qiagen (Valencia, CA, USA). Protein assay reagents, acrylamide, bis-acrylamide, TEMED, and ammonium persulfate were acquired from Bio-Rad Laboratories (Hercules, CA, USA). Unless otherwise indicated, all other chemicals were commercial products of analytical or molecular biological grade.

Enzyme expression and purification

To express His_6-tagged *Bl*ALDH, *E. coli* M15 cells carrying pQE-*ybcD* (Lo and Chen 2010) were grown aerobically in 100-mL LB medium supplemented with the antibiotics ampicillin (100 μg/mL) and kanamycin (25 μg/mL) until OD_{600} reached 1.0. Isopropyl-β-D-thiogalactopyranoside was added to a final concentration of 0.1 mM, and the culture was cultivated at 37°C in a shaking incubator for another 12 h. Cells were then harvested by centrifugation, resuspended in 3 mL of binding buffer (5 mM imidazole, 0.5 M NaCl, and 50 mM NaH_2PO_4; pH 7.9), and sonicated on ice (30-s bursts and pulses for 5 min). After removal of cell debris by centrifugation, the recombinant enzyme was purified by affinity chromatography with a Ni^{2+}-NTA agarose column (Qiagen) under native conditions.

Gel electrophoresis and determination of protein concentration

Polyacrylamide gel electrophoresis (PAGE) was carried out in a mini-Protean III system (Bio-Rad Laboratories) with a 10% non-denaturing polyacrylamide gel. Electrophoresis was done at ambient temperature and a constant voltage of 100 V for 4 h. Sodium dodecyl sulfate-PAGE (SDS-PAGE) was performed using the Laemmli buffer system (1970). The gels were stained with 0.25% (w/v) Coomassie brilliant blue R-250 dissolved in 50% (v/v) methanol-10% (v/v) acetic acid, and destained by a solution of 30% (v/v) methanol and 10% (v/v) acetic acid.

Protein concentrations were measured with the Bio-Rad protein assay reagent, and bovine serum albumin was used as the protein standard.

Activity assay

*Bl*ALDH activity was assayed by the procedure described previously (Lo and Chen 2010). Firstly, the reaction mixture containing 50 mM potassium phosphate buffer (pH 7.0), 1 mM DTT, 2 mM propionaldehyde, and 4 mM NAD^+ was equilibrated at 37°C for 5 min. The reaction was initiated by adding 3.4 μg/mL enzyme. Following incubation at the same temperature for 20 min, enzyme activity was measured by monitoring the reduction of NAD^+ to NADH at 340 nm, and the amount of NADH formed was determined with $\Delta\varepsilon_{340} = 6.22\ \mathrm{mM}^{-1}\ \mathrm{cm}^{-1}$. One unit of *Bl*ALDH activity was defined as the amount of enzyme required to reduce 1 μmol of NAD^+ to NADH in 1 min. All enzyme assays were performed in triplicate.

Analytical ultracentrifugation

A Beckman Optima XL-A analytical ultracentrifuge device (Fullerton, CA, USA) was used to perform the sedimentation velocity experiments. *Bl*ALDH (370 μL) and 50 mM phosphate buffer (400 μL; pH 7.0) solutions were loaded into the double sector centerpiece separately and established in a Beckman An-50 Ti rotor. A rotor speed of 42,000 rpm and a rotor temperature of 20°C were used in the sedimentation velocity experiments. The UV absorption of the cell at 280 nm was scanned in a continuous mode with time interval of 8 min and step size of 3 mm. The partial specific volume of the enzyme, solvent density, and viscosity were calculated by the software SEDNTERP (http://www.jphilo.mailway.com/). The protein sample was visually checked for clarity after centrifugation to make sure that there was no indication of precipitation. The recorded scans at different time points were collected and fitted to a continuous size distribution model using the SEDFIT program (Schuck 2000; Brown and Schuck 2006).

The observed sedimentation profile of a continuous size distribution [$c(s)$] can be calculated from Eq. 1:

$$a(r,t) = \int c(s)\chi(s, D(s), r, t)\mathrm{d}s + \varepsilon \tag{1}$$

where $a(r, t)$ denotes the observed sedimentation data, $c(s)$ represents the concentration of species with sedimentation coefficients between s and $s + \mathrm{d}s$, and $\chi(s, D(s), r, t)$ is the solution of Lamm equation. The Lamm equation and the molecular parameters that determine the s-value are given by Eqs. 2 and 3, respectively.

$$\frac{\partial\chi(r,t)}{\partial t} = \frac{1}{r}\frac{\partial}{\partial r}\left[rD\frac{\partial\chi(r,t)}{\partial r} - s\omega^2 r^2\chi(r,t)\right] \tag{2}$$

$$s = \frac{u}{\omega^2 r} = \frac{M(1-\bar{v}\rho)}{N_A f} = \frac{\mathrm{MD}(1-\bar{v}\rho)}{\mathrm{RT}} \tag{3}$$

where ω denotes angular velocity, T is absolute temperature, u is the observed radial velocity of the macromolecule, ω is the angular velocity of the rotor, r is the radial position, $\omega^2 r$ is the centrifugal field, M is the molar mass, $\bar{v}$ is the partial specific volume, ρ is the density of the solvent, N_A is Avogadro's number, and f is the gas constant. The relationship $D = \mathrm{RT}/N_A f$ is used to obtain the right-hand version of the Svedberg equation.

The sedimentation velocity data were also fitted using a two-dimensional distribution with respect to frictional ratio $c(s, f/f_o)$ according to Eq. 4 (Schuck 2000):

$$a(r,t) = \iint c(s,f/f_0)\chi(s, D(s,f/f_0), r, t)dsd(f/f_0) \tag{4}$$

with $a(r, t)$ denoting the observed optical signal at radius r and time t; $\chi(s, D, r, t)$, the solution of the Lamm equation; and $D(s, f/f_o)$, the dependence of diffusion coefficient (D) on sedimentation coefficient (s) and frictional ratio (f/f_o).

Circular dichroism spectroscopy

CD spectra in the far UV region (190–250 nm) were recorded on a JASCO model J-815 equipped with Peltier thermostated cuvette holder under constant nitrogen flow. The photomultiplier absorbance was always below 600 V in the analyzed region. Each scanning was repeated ten times, and an average was reported. Data were corrected for the buffer effect, and the experimental results were expressed as molar ellipticity [θ] in the units of degrees·cm^2·dmol^{-1} according to Eq. 5:

$$[\theta] = \frac{\theta}{10 \cdot C \cdot l} \tag{5}$$

where l represents the light path length (cm), C is the molar concentration of protein (mol/L), and θ denotes the observed ellipticity (mdeg).

The unfolding transition curves for *Bl*ALDH were obtained by monitoring the ellipticity at 222 nm in a 1-mm cell. The temperature was increased at heating rates of 1, 4, and 8°C/min from 20 to 100°C, and the transition mid point (T_m) was recorded. For refolding experiments, the cooling rates of 1, 4, and 8°C/min were employed, and measurements were taken every minute.

Fluorescence spectroscopy

Fluorescence spectra of the recombinant enzyme were monitored at 30°C in a Hitachi F-7000 fluorescence spectrophotometer with an excitation wavelength of 280 nm. All spectra were corrected for buffer absorption. The fluorescence emission spectra of protein samples with a concentration of 36.4 μM were recorded from 300 to 400 nm at a scanning speed of 240 nm/min. The maximum peak of the fluorescence spectrum and the change in fluorescence intensity were used in monitoring the unfolding processes of the enzyme. Both the red shift and the change in fluorescence intensity were analyzed together using the average emission wavelength (AEW) (λ) according to Eq. 6 (Royer et al. 1993):

$$\langle\lambda\rangle = \frac{\sum_{i=\lambda_1}^{\lambda_N}(F_i \cdot \lambda_i)}{\sum_{i=\lambda_1}^{\lambda_N} F_i} \quad (6)$$

in which F_i is the fluorescence intensity at the specific emission wavelength (λ_i).

Unfolding of the recombinant enzyme by chemical denaturants

The unfolding experiments of *Bl*ALDH were examined in different concentrations of GdnHCl and urea in 50 mM phosphate buffer (pH 7.0) at ambient temperature. The preliminary experiments showed that 30-min incubation time was sufficient for the unfolding to achieve equilibrium under all denaturant concentrations.

The unfolding curves of *Bl*ALDH were used to calculate the thermodynamic parameters by global fitting of the experimental data. The two-state unfolding model (Scheme 1) is described by Eq. 7 (Pace 1990):

$$y_{obs} = \frac{(y_N + m_f[D]) + (y_U + m_u[D]) \cdot \exp[-(\Delta G_{H_2O} - m[D])/RT]}{1 + \exp[-(\Delta G_{H_2O} - m[D])/RT]} \quad (7)$$

where y_{obs} is the observed biophysical signal, y_N and y_U are the intercepts, m_f and m_u are the slopes of the pre- and post-transition baselines, T is temperature, R is the universal gas constant, [D] is the concentration of urea and GdnHCl, ΔG_{H_2O} represents an estimate of the conformational stability of the protein in the absence of denaturant, and m is a measure of the dependence of ΔG.

$$N \xleftrightarrow{K_{N-U}} U$$

Scheme 1 Two-state folding/unfolding process

Results and discussion

Quaternary structure of the purified enzyme

Proteins are one of the most common and important cellular macromolecules and control almost all biological processes. Every protein of living organisms acquires a unique conformation in order to be functionally effective. To determine the biophysical properties of *Bl*ALDH, the recombinant enzyme in the crude extract of IPTG-induced *E. coli* M15 (pQE-*ybcD*) was purified to near homogeneity using Ni^{2+}-NTA resin. SDS-PAGE analysis revealed that the subunit mass of *Bl*ALDH was approximately 53 kDa (Fig. 1a). The purification procedure resulted in a protein yield of about 24%, and the purified enzyme had a specific

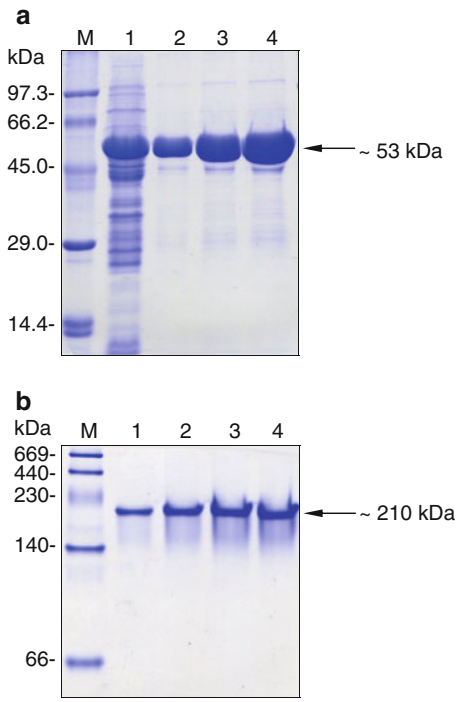

Fig. 1 Gel electrophoresis analysis of the purified *Bl*ALDH. **a** SDS-PAGE analysis. Lanes: *M* protein size marker; *1* the cell-free extract of *E. coli* M15 (pQE-*ybcD*); *2* elution fraction 1; *3* elution fraction 2; *4* elution fraction 3. **b** Native-PAGE analysis. Lanes: *M* protein size marker; *1* 1.2 μg of the purified enzyme; *2* 2.4 μg of the purified enzyme; *3* 3.6 μg of the purified enzyme; *4* 4.8 μg of the purified enzyme

activity of 106.5 ± 9.4 U/mg protein. Additionally, the molecular size of native *Bl*ALDH was approximately 210 kDa as estimated from the nondenaturing gel (Fig. 1b), suggesting that the enzyme exists as a tetramer.

Quaternary structure of biomolecules has piqued recent interest in the literature due to its potential modulation of protein dynamics (Benkovic et al. 2008; Burgess et al. 2008; Cansu and Doruker 2008), which are increasingly recognized as being crucial for enzyme catalysis. As recombinant DNA techniques have now made many macromolecules available for investigation on the 10–100 mg level, there has been a renewed interest in understanding the structure–function relationship of different kinds of protein molecules. Among the analytical methods for defining macromolecular assemblies, AUC is experiencing a renaissance due largely to the availability of modern computer-based instrumentation and its resulting expanded applications (Laue and Statford 1999; Lebowitz et al. 2002). In this regard, the oligomeric state of *Bl*ALDH (0.74 mg/mL) was examined by AUC. As shown in Fig. 2, the protein molecule sediments at 10.5 ± 0.3 S correspond to a species with a molar mass of 231,000 ± 5,000 Da, which is in agreement with the 210.728-kDa molecular mass calculated from the amino acid sequence of a tetramer. The AUC data also indicate that the tetramer is an exclusive form of *Bl*ALDH at protein concentrations up to 1.5 mg/mL (data not shown). The excellent matching between the experimental data and the fitted curve (Fig. 2a), the homogeneous bitmap picture (data not shown), and the randomly distributed residual values (Fig. 2b) all demonstrated that a highly reliable model for the sedimentation velocity experiments was obtained and AUC was an excellent biophysical probe for evaluating the molecular structure of *Bl*ALDH.

The self-assembly of proteins plays a vital role in the catalytic function of a variety of enzymes, such as tryparedoxin peroxidase of *Trypanosoma cruzi* (Yuan et al. 2010), flavin adenine dinucleotide synthetase of

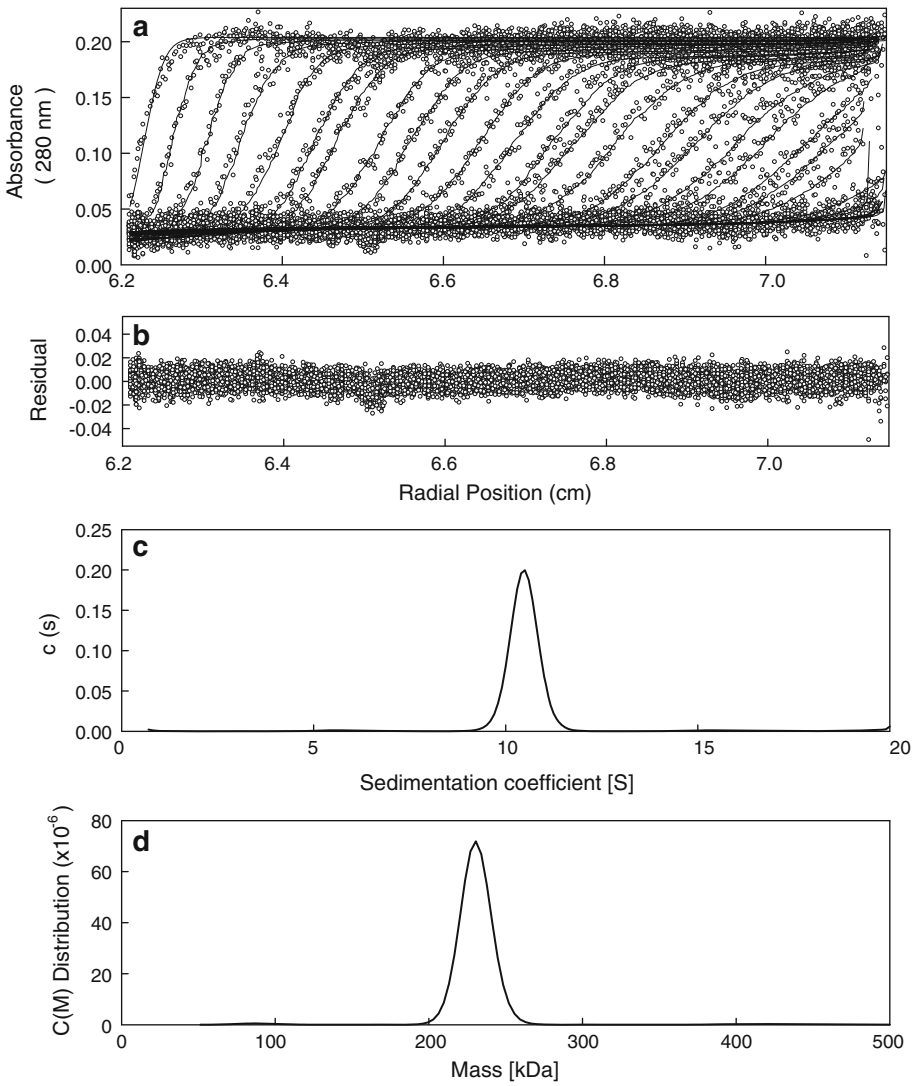

Fig. 2 Sedimentation velocity experiments of *Bl*ALDH. **a** A typical trace of absorbance at 280 nm of the recombinant enzyme during the sedimentation velocity experiment. The *symbols* are experimental data, and the *lines* are computer-generated results by fitting the experimental data to the Lamm equation with SEDFIT program. **b** The residuals of the model fitting of the data in panel **a**. **c** The continuous sedimentation coefficient distribution of the recombinant enzyme at a protein concentration of 0.74 mg/mL. **d** The continuous molar mass distribution of the recombinant enzyme

Corynebacterium ammoniagenes (Herguedas et al. 2010), heme oxygenase-1 of endoplasmic reticulum (Hwang et al. 2009), Sin resolvase of *Staphylococcus aureus* (Mouw et al. 2010), dihydrofolate reductase of *Thermotoga maritima* (Loveridge et al. 2009), and γ-cyclodextrin-specific cyclodextrinase of *Bacillus clarikii* (Nakagawa et al. 2008). Although an extended loop structure in ALDHs of *Vibrio harveyi* (Ahvazi et al. 2000) and *Burkholderia xenovorans* (Bains and Boulanger 2008) definitely prevents their further multimerization to form the "dimer of dimers," X-ray crystal structures of sheep liver cytosolic ALDH (Moore et al. 1998), *Streptococcus mutans* ALDH (Cobessi et al. 1999), *E. coli* ALDH (Di Costanzo et al. 2007), and human liver mitochondrial ALDH (Ni et al. 1999) have all shown that these enzymes exist as a homotetramer. Consistently, the native-PAGE and AUC data clearly indicate that the homotetramer is a predominant form of *Bl*ALDH in solution (Figs. 1b and 2). However, it should be noted that protein assembly is a concentration-dependent event that enhances logarithmically with an increase in biomolecule concentration. Many enzymes are found to confer an interconvertible mixture of monomers and oligomers (Lunn et al. 2008; Gruber et al. 2009; Dengra-Pozo et al. 2009). Although our findings cannot directly address whether the SDR family enzymes form active dimers or tetramers, we reported that *Bl*ALDH, a typical member of the SDR superfamily, exists in solution as a tetramer. These findings confirm the previous results of gel filtration experiments (Lo and Chen 2010).

Importantly, the AUC data also allowed us to calculate the frictional ratio (f/f_o) of *Bl*ALDH. Frictional ratio is a measure of the degree of asymmetry in a biomolecule with respect to an anhydrous sphere of the same mass. For approximately globular proteins, this value lies in the range of 1.05–1.32 (Smith 1988). By fitting the AUC data with Eq. 4, a frictional ratio of 1.28 was obtained for *Bl*ALDH. This result demonstrates that the enzyme is basically a spherical protein molecule in solution.

Effects of sodium dodecyl sulfate and organic solvents on the *Bl*ALDH structure

SDS, an anionic surfactant, has been shown to unfold and inactivate creatine kinase (Wang et al. 1995), aminoacylase (He et al. 1995), and α-amylases (Chakraborty et al. 2009; Shafiei et al. 2011). This surfactant is frequently used to denature protein samples for SDS-PAGE analysis (Chrambach and Rodbard 1971). In the fully denatured protein, it can specifically or non-cooperatively bind to proteins at a high molecule ratio (Reynolds and Tanford 1970) and, in some cases, may even activate enzymes (Jones et al. 1987; Moore and Flurkey 1990). In this study, the effect of SDS on *Bl*ALDH activity was studied. The residual activity was determined after incubating the 5% SDS-enzyme solution at 25°C for 30 min. As shown in Fig. 3a, *Bl*ALDH activity was appreciably affected by the presence of SDS, with

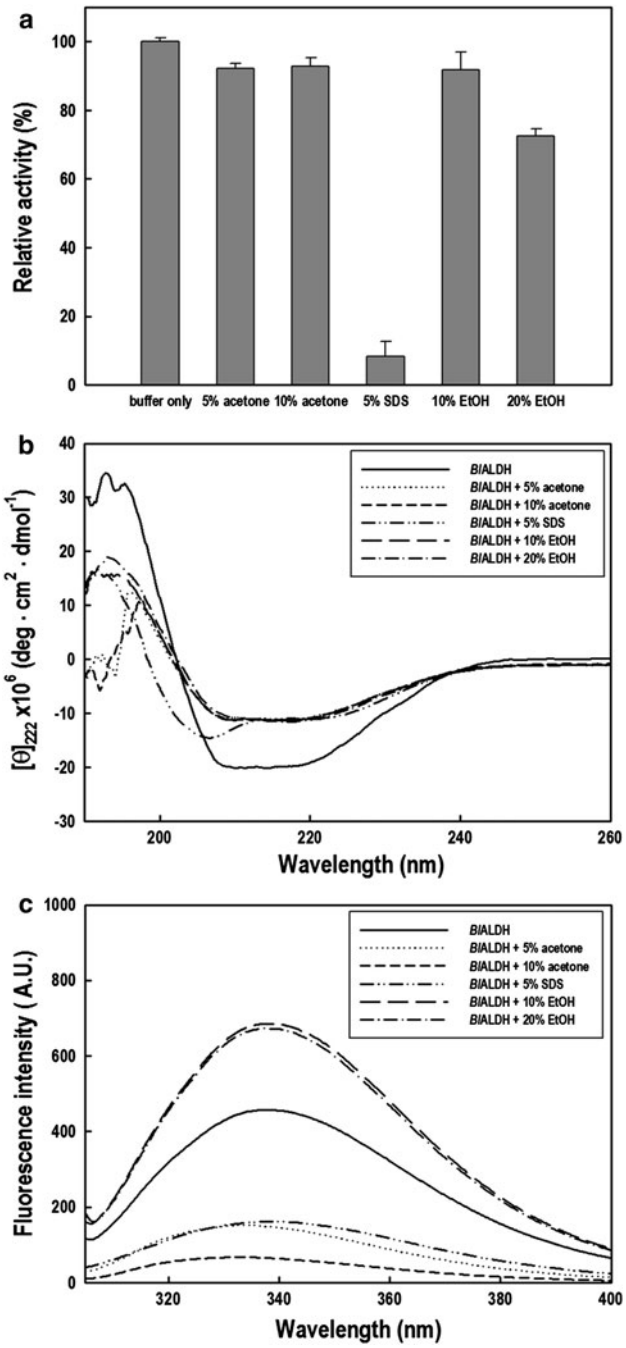

Fig. 3 Influence of environmental variables on the enzymatic activity, and the far-UV CD and fluorescence spectra of *Bl*ALDH. **a** Effects of SDS and organic solvents on the enzymatic activity. The enzyme was incubated with the desired environmental variable for 30 min at 25°C and the residual activity was monitored under the standard assay conditions. **b** and **c** Effects of SDS and organic solvents on the far-UV CD and fluorescence spectra of the enzyme. Far-UV CD (**b**) and fluorescence (**c**) spectra were obtained with protein concentration of approximately 0.2 mg/mL

approximately 8.4% of the activity remaining. Considering that SDS could bind to *Bl*ALDH enzyme with more than one binding site, both the modified structure and altered charge distribution induced by the specific binding of this surfactant might be responsible for the inhibition.

Water-miscible organic solvents, such as acetone and ethanol, are used in industry to produce a wide range of chemicals and are frequently present in wastewaters (Grodowska and Parczewski 2010). Given that *Bl*ALDH might be employed in the treatment of aldehyde-containing wastewater, effects of acetone and ethanol on the enzymatic activity were therefore determined. After 30 min incubation at 25°C, the residual activity was monitored under standard assay conditions (Fig. 3a). Apparently, *Bl*ALDH was stable in the presence of 5–10% acetone, and the activity was only slightly inhibited by 20% ethanol. The maintenance of protein conformation over a wide concentration range of water-miscible organic solvents has been reported for other enzymes, such as thermolysin (English et al. 1999) and neutral protease (Mansfeld and Ulbrich-Hofmann 2007).

To analyze the secondary structures of *Bl*ALDH, far-UV CD measurements were performed under various conditions. The CD spectrum of *Bl*ALDH displays strong peaks of negative ellipticity at 208 and 222 nm, indicative of substantial α-helical contents (Fig. 3b). Obviously, SDS had a marked effect on the secondary structures of *Bl*ALDH (Fig. 3b). This might be the reason for the abolishment of *Bl*ALDH activity by 5% SDS. However, no profound alteration in the CD spectra together with a significant decrease in the fluorescence intensity were observed in the presence of 5–10% acetone (Fig. 3b and c), indicating that the tertiary structure of *Bl*ALDH was changed upon the addition of this solvent. Organic-solvent-tolerant enzymes appear to be quite attractive for commercial applications such as bioremediation of industrial wastewaters contaminated with organic solvents. The organic-solvent-tolerant characteristic has been reported in α-amylases from *Haloarcula* sp. strain S-1 (Fukushima et al. 2005) and *Nesterentonia* sp. strain F (Shafiei et al. 2011), proteases from *Pseudomonas aeruginosa* (Rahman et al. 2005; Tang et al. 2008) and *B. licheniformis* (Rachadech et al. 2010), and glucose 1-dehydrogenase from *Lysinibacillus sphaericus* (Ding et al. 2010). Interestingly, the fluorescence intensity was increased to more than 33.2% of the original upon the addition of 10–20% ethanol. Based on the fact that *Bl*ALDH was still active in the presence of ethanol (Fig. 3a), more studies are required to elucidate the reason of this finding.

Thermal unfolding of the recombinant enzyme

Thermal unfolding of *Bl*ALDH was followed by monitoring the ellipticity at 222 nm under constant heating rates. Figure 4 shows the transition curves obtained from

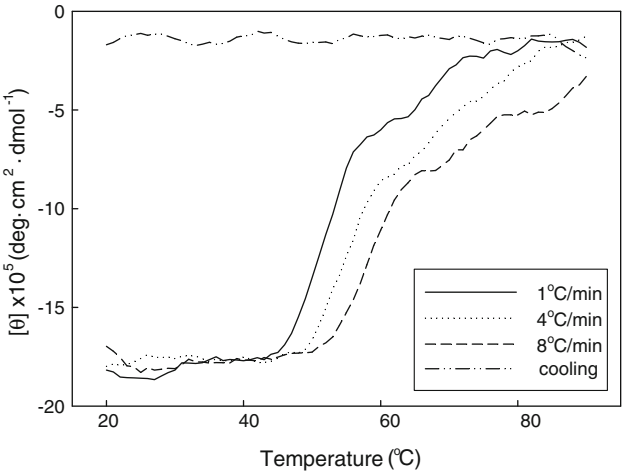

Fig. 4 Heating and cooling profiles of *Bl*ALDH in 50 mM potassium phosphate buffer (pH 7.0). Transitions were obtained by recording the ellipticity of this enzyme at 222 nm

*Bl*ALDH solutions at heating rates of 1, 4, and 8°C/min. As compared with the heating rates of 4 and 8°C/min, the thermal transition for 1°C/min appeared at lower temperature. This finding resembles the experimental result for transitions under kinetic control (Freire et al. 1990). Also, the lower heating rate resulted in larger changes in the far-UV CD transition, probably indicating aggregation of *Bl*ALDH. The impact of heating rates on the apparent transition temperatures has been demonstrated in a variety of proteins (Galisteo et al. 1991; Lepock et al. 1992; Plaza del Pino et al. 2000; Vogl et al. 1997).

To further explore if the unfolding reaction was reversible or not, the sample was heated at a constant heating rate. After the thermal denaturation transitions went to completion, the enzyme solutions were cooled down to 20°C at the same scan speed. Figure 4 shows the cooling curve of *Bl*ALDH at a heating rate of 1°C/min. It is clear that the secondary structures of the native polypeptide were not recovered after the sample was cooled down to the indicated temperature. Similarly, no detectable recovery in the secondary structures was observed for other heating rates (data not shown). These results indicate that thermal unfolding of *Bl*ALDH is highly irreversible. The irreversible process seems to be the more common case for most proteins, such as peroxidase (Zamorano et al. 2009), triose phosphate isomerase (Shi et al. 2008), α-amylase (Duy and Fitter 2005), L-2-hydroxyisocaproate dehydrogenase (Bao et al. 2007), and latex amine oxidase (Amani et al. 2007).

Guanidine hydrochloride- and urea-induced unfolding

GdnHCl- and urea-induced unfolding of *Bl*ALDH was investigated. Time-dependent changes in the structural properties and dehydrogenase activity of this enzyme in

0–6 M GdnHCl and 0–8 M urea were monitored to standardize the incubation time required to achieve equilibrium. Under the conditions studied, the changes occurred within a maximum of 30 min for GdnHCl and urea, with no further alterations in the values obtained up to 12 h (data not shown). These observations suggest that a minimum time of 30 min is sufficient to achieve the equilibrium.

Enzymatic activity can be regarded as the most sensitive probe to study the changes in enzyme conformation during various treatments because it reflects subtle readjustments at the active site, enabling very small conformational variations of an enzyme structure to be detected. The effect of increasing concentrations of GdnHCl on the dehydrogenase activity of *Bl*ALDH is summarized in Fig. 5a. The recombinant enzyme treated with 0.4 M GdnHCl retained >80% of the dehydrogenase activity. An increase in concentration up to 1 M resulted in a complete loss of the activity. These results reveal that the GndHCl concentration below 0.4 M induces minor changes, probably in and around the active site.

GdnHCl-induced unfolding of *Bl*ALDH was performed to explore the effect of this denaturant on the secondary structures of the enzyme. The effect of increasing GdnHCl concentrations on the ellipticity of *Bl*ALDH at 222 nm is illustrated in Fig. 5b. Obviously, the secondary structures of *Bl*ALDH were very sensitive to GdnHCl treatment. A large decrease in the negative ellipticity was observed at GdnHCl concentrations between 0.1 and 1.2 M, indicating a significant disruption in the secondary structures of the enzyme under these conditions. By fitting with Eq. 6, *Bl*ALDH showed $[GdnHCl]_{0.5,N-U}$ of 0.67 M, corresponding to a free energy change of 1.37 kcal/mol for the N → U process.

Fluorescence spectra provide a sensitive means to characterize proteins and their conformations. The spectrum is determined mainly by the polarity of the environment of the tryptophan and tyrosine residues and by their specific interactions (Royer 2006). In this regard, AEW, which reports the changes in both fluorescence wavelength and intensity, was used to calculate the thermodynamic parameters of the unfolding process. For *Bl*ALDH, the AEW values in the absence of GdnHCl and at GdnHCl concentrations >2 M were 345.6 and 352.1 nm, respectively. The transition occurred at 0.93 M GdnHCl and a plateau region existed from 2.2 to 6 M (Fig. 5c). The tryptophan emission λ_{max} of 347.8 nm was observed after treatment of *Bl*ALDH with 6 M GdnHCl. Normally exposed tryptophan in the unfolded protein shows emission λ_{max} between 340 and 356 nm (Lakowicz 1999), indicating that incubation of *Bl*ALDH with a higher concentration of GdnHCl leads to significant unfolding of the protein molecule.

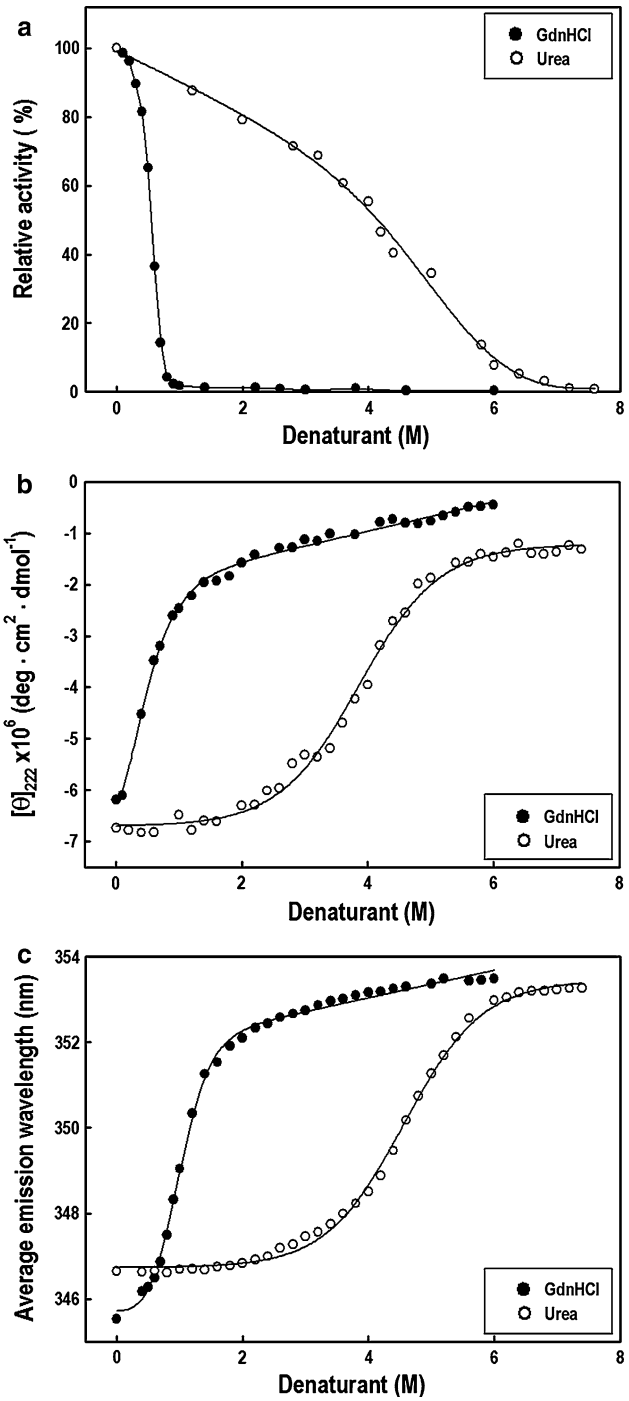

Fig. 5 GdnHCl- and urea-induced denaturation of *Bl*ALDH. **a** Change in enzymatic activity of *Bl*ALDH with increasing concentrations of GdnHCl or urea. The recombinant enzyme was incubated with the desired concentration of GdnHCl or urea for 30 min at ambient temperature, and the dehydrogenase activity was measured under the standard assay conditions. *Bl*ALDH activity observed in the absence of the denaturant was taken as 100%. **b** GdnHCl- and urea-induced changes in the secondary structures of *Bl*ALDH as monitored by the negative ellipticity of the protein sample at 222 nm. **c** GdnHCl- and urea-induced changes in the AEW value of *Bl*ALDH

Although urea and GdnHCl are believed to have a similar mode of action (Pace 1990), GdnHCl is a monovalent salt that has both ionic and chaotropic effects but urea has only chaotropic effects (Monera et al. 1994). Thus, urea is an ideal control agent to distinguish between the ionic and chaotropic effects of GdnHCl. The effect of increasing concentration of urea on the dehydrogenase activity of *Bl*ALDH was therefore investigated. As shown in Fig. 5a, more than 80% of the *Bl*ALDH activity was retained at concentrations of urea up to 2 M. A sharp decrease in *Bl*ALDH activity was observed when urea concentrations were set between 3 and 6 M, and the activity was abolished completely at concentrations greater than 6.6 M.

The effect of increasing urea concentrations on the secondary structures of *Bl*ALDH was studied by monitoring changes in ellipticity at 222 nm. As shown in Fig. 5b, only a slight decrease (approximately 8%) in the negative ellipticity occurred when the urea concentration was increased up to 3.0 M. However, a rapid decrease in the negative ellipticity was observed at urea concentrations between 3.2 and 5.6 M. By fitting with Eq. 6, *Bl*ALDH showed $[\text{urea}]_{0.5,\text{N–U}}$ of 4.03 M, corresponding to a free energy change of 3.45 kcal/mol for the N → U process.

The urea-induced unfolding of *Bl*ALDH was also demonstrated by tryptophan fluorescence studies as the urea concentration increased. As shown in Fig. 5c, the fluorescence signal of urea-induced *Bl*ALDH followed a monophasic process, and the enzyme started to unfold at 2.2 M denaturant with $[\text{urea}]_{0.5\ \text{N–U}}$ of 4.69 M. Low concentration of urea did not induce the change in the AEW value of *Bl*ALDH, whereas the tryptophan residues in the protein were highly exposed to the buffer environment at values above 6 M, allowing us to consider the protein completely unfolded.

Taken together, *Bl*ALDH is more stable against the unfolding action of urea but not against GdnHCl. It has been reported that GdnHCl is ~2 times more effective as a denaturant than urea in the unfolding of proteins (Vecchio et al. 2002). Consistently, GdnHCl is ~4 times more effective than urea in the unfolding of *Bl*ALDH. Usually, $[\text{urea}]_{0.5\ \text{N–U}}$ reveals the net stability of the protein contributed by hydrophobic and electrostatic interactions (Monera et al. 1994). Although the exact molecular mechanism of the denaturing action of GdnHCl and urea has not been clearly defined (Schellman 2002), it was presumed that both denaturant molecules unfold proteins by solubilizing the non-polar parts along with the polar groups in the side chains of the protein molecules (Nandi and Robinson 1984). The unfolding of *Bl*ALDH might follow the same path with both denaturants; however, more studies are required to elucidate their different effects on the unfolding process of *Bl*ALDH.

Conclusion

To our knowledge, this study represents the first biophysical characterization of an $NAD(P)^+$-dependent short-chain ALDH from an industrially important bacterium. The remarkable resistance of *Bl*ALDH towards water-miscible organic solvents constitutes evidence of the sturdiness of this biocatalyst and suggests exploratory investigations on conversion of poorly water-soluble substrates in a biphasic reaction media. Moreover, biophysical studies of this enzyme provide more information for the inherent quaternary structure of the SDR superfamily enzymes and contribute to a better understanding of their enzymatic properties, especially a fuller appreciation of the structure–activity relationship at molecular level.

Acknowledgments The authors are grateful to Dr. Hui-Chih Hung for providing the necessary facilities to carry out the AUC experiments. This work was supported by a research grant (NSC 97-2628-B-415-001-MY3) from National Science Council of Taiwan.

References

Ahvazi B, Coulombe R, Delarge M, Vedadi M, Zhang L, Meighen E, Vrielink A (2000) Crystal structure of the $NADP^+$-dependent aldehyde dehydrogenase from *Vibrio harveyi*: structural implications for cofactor specificity and affinity. Biochem J 349:853–861

Amani M, Moosavi-Movahedi AA, Floris G, Kurganov BI, Almad F, Saboury AA (2007) Two-state irreversible thermal denaturation of *Euphorbia characias* latex amine oxidase. Biophys Chem 125:254–259

Bains J, Boulanger MJ (2008) Structural and biochemical characterization of a novel aldehyde dehydrogenase encoded by the benzoate oxidation pathway in *Burkholderia xenovorans* LB400. J Mol Biol 379:597–608

Bao L, Chatterjee S, Lohmer S, Schomburg D (2007) An irreversible and kinetically controlled process: thermal induced denaturation of L-2-hydroxyisocaproate dehydrogenase from *Lactobacillus confuses*. Protein J 26:143–151

Benkovic SJ, Hammes GG, Hammes-Schiffer S (2008) Free-energy landscape of enzyme catalysis. Biochemistry 47:3317–3321

Birrer GA, Cromwick AM, Gross RA (1994) Gamma-poly(glutamic acid) formation by *Bacillus licheniformis* 9945a: physiological and biochemical studies. Int J Biol Macromol 16:265–275

Brown PH, Schuck P (2006) Macromolecular size-and-shape distributions by sedimentation velocity analytical ultracentrifugation. Biophys J 90:4651–4661

Burgess BR, Dobson RCJ, Bailey MF, Atkinson SC, Griffin MDW, Jameson GB, Parker MW, Gerrard JA, Perugini MA (2008) Structure and evolution of a novel dimeric enzyme from a clinically important bacterial pathogen. J Biol Chem 283:27598–27603

Cabellero A, Baldoma L, Ros J, Boronat A, Aguilar J (1983) Identification of lactaldehyde dehydrogenase and glycolaldehyde dehydrogenase as functions of the same protein in *Escherichia coli*. J Biol Chem 258:7788–7792

Cansu S, Doruker P (2008) Dimerization affects collective dynamics of triosephosphate isomerase. Biochemistry 47:1358–1368

Chakraborty S, Khopade A, Kokarc C, Mahadik K, Chopade B (2009) Isolation and characterization of novel α-amylase from marine *Streptomyces* sp. D1. J Mol Catal B Enzym 58:17–23

Chrambach A, Rodbard D (1971) Polyacrylamide gel electrophoresis. Science 172:440–451

Cobessi D, Tete-Favier F, Marchal S, Azza S, Branlant G, Aubry A (1999) Apo and holo crystal structures of an NADP-dependent aldehyde dehydrogenase from *Streptococcus mutans*. J Mol Biol 290:161–173

Dengra-Pozo J, Martinez-Rodriguez S, Contreras LM, Prieto J, Andujar-Sanchez M, Clemente-Jimenez JM, Las Heras-Vazquez FJ, Rodriguez-Vico F, Neira JL (2009) Structure and conformational stability of a tetrameric thermostable *N*-succinylamino acid racemase. Biopolymers 91:757–772

Di Costanzo L, Gomez GA, Christianson DW (2007) Crystal structure of lactaldehyde dehydrogenase from *Escherichia coli* and inferences regarding substrate and cofactor specificity. J Mol Biol 366:481–493

Dickinson FM, Haywood GW (1986) The effects of Mg^{2+} on certain steps in the mechanisms of the dehydrogenase and esterase reactions catalysed by sheep liver aldehyde dehydrogenase: support for the view that dehydrogenase and esterase activities occur at the same site on the enzyme. Biochem J 233:877–883

Ding HT, Du YQ, Liu DF, Li ZL, Chen XJ, Zhao YH (2010) Cloning and expression in *E. coli* of an organic solvent-tolerant and alkali-resistant glucose 1-dehydrogenase from *Lysinibacillus sphaericus*. Bioresour Technol 102:1528–1536

Duy C, Fitter J (2005) Thermostability of irreversible unfolding α-amylases analyzed by unfolding kinetics. J Biol Chem 280:37360–37365

English AC, Done SH, Caves LSD, Groom CR, Hubbard RE (1999) Locating interaction sites on proteins: the crystal structure of thermolysin soaked in 2% to 100% isopropanol. Proteins 37:628–640

Feldman RI, Weiner H (1972) Horse liver aldehyde dehydrogenase: purification and characterization. J Biol Chem 247:260–266

Freire E, van Osdol WW, Mayorga OL, Sanchez-Ruiz JM (1990) Calorimetrically determined dynamics of complex unfolding transitions in proteins. Annu Rev Biophys Biophys Chem 19:159–188

Fukushima T, Mizuki T, Echigo A, Inoue A, Usami R (2005) Organic solvent tolerance of halophilic α-amylase from a *Haloarchaeon*, *Haloarcula* sp. strain S-1. Extremophiles 9:85–89

Galisteo ML, Mateo PL, Sanchez-Ruiz JM (1991) Kinetic study on the irreversible thermal denaturation of yeast phosphoglycerate kinase. Biochemistry 30:2061–2066

Grodowska K, Parczewski A (2010) Organic solvents in pharmaceutical industry. Acta Plo Pharm 67:3–12

Gruber CW, Cemazar M, Mechler A, Martin LL, Crail DJ (2009) Biochemical and biophysical characterization of a novel plant protein disulfide isomerase. Peptide Sci 92:35–43

Hanlon SP, Hill TK, Flavell MA, Stringfellow JM, Cooper RA (1997) 2-Phenylethylamine catabolism by *Escherichia coli* K-12: gene organization and expression. Microbiology 143:513–518

Hart GJ, Dickinson FM (1982) Kinetic properties of highly purified preparations of sheep liver cytoplasmic aldehyde dehydrogenase. Biochem J 203:617–627

He B, Zhang Y, Zhang T, Wang HR, Zhou HM (1995) Inactivation and unfolding of aminoacylase during denaturation in sodium dodecyl sulfate solutions. J Protein Chem 14:349–357

Hempel J, Perozich J, Chapman T, Rose J, Boesch JS, Liu ZJ, Lindahl R, Wang BC (1999) Aldehyde dehydrogenase catalytic mechanism: a proposal. Adv Exp Med Biol 463:53–59

Hempel J, Kuo I, Perozich J, Wang BC, Lindahl R, Nicholas H (2001) Aldehyde dehydrogenase: maintaining critical active site geometry at motif 8 in the class 3 enzyme. Eur J Biochem 268:722–726

Herguedas B, Martínez-Júlyez M, Frago S, Medina M, Hermoso JA (2010) Oligomeric state in the crystal structure of modular FAD synthetase provides insights into its sequential catalysis in prokaryotes. J Mol Biol 400:218–230

Ho KK, Weiner H (2005) Isolation and characterization of an aldehyde dehydrogenase encoded by *aldB* gene of *Escherichia coli*. J Bacteriol 187:1067–1073

Hsu LC, Chang WC, Shibuya A, Yoshida A (1992) Human stomach aldehyde dehydrogenase cDNA and genomic cloning, primary structure, and expression in *Escherichia coli*. J Biol Chem 267:3030–3037

Hurley TD, Steinmetz CG, Weiner H (1999) Three-dimensional structure of mitochondrial aldehyde dehydrogenase: mechanistic implications. Adv Exp Med Biol 463:15–25

Hwang HW, Lee JR, Chou KY, Suen CS, Hwang MJ, Chen C, Shieh RC, Chau LY (2009) Oligomerization is crucial for the stability and function of heme oxygenase-1 in the endoplasmic reticulum. J Biol Chem 284:22672–22679

Johansson K, El-Ahmad M, Ramaswamy S, Hjelmqvist L, Jornvall H, Eklund H (1998) Structure of betaine aldehyde dehydrogenase at 2.1 Å resolution. Protein Sci 7:2106–2117

Jones MN, Finn A, Mosavi-Movahedi A, Waller BJ (1987) The activation of *Aspergillus niger* catalase by sodium *n*-dodecylsulphate. Biochim Biophys Acta 913:395–398

Laemmli UK (1970) Cleavage of structural proteins during the assembly of the head of bacteriophage T4. Nature 227:680–685

Lakowicz JR (1999) Principles of fluorescence spectroscopy, 2nd edn. Kluwer Academic, New York

Lamb AL, Newcomer ME (1999) The structure of retinal dehydrogenase type II at 2.7 Å resolution: implications for retinal specificity. Biochemistry 38:6003–6011

Laue TM, Statford WF (1999) Modern applications of analytical ultracentrifugation. Annu Rev Biophys Biomol Struct 28:75–100

Lebowitz J, Lewis MS, Schuck P (2002) Modern analytical ultracentrifugation in protein science: a tutorial review. Protein Sci 11:2067–2079

Lepock JR, Ritchie KP, Kolios MC, Rodahl AM, Heinz KA, Kruuv J (1992) Influence of transition rates and scan rate on kinetic simulations of differential scanning calorimetry profiles of reversible and irreversible protein denaturation. Biochemistry 31:12706–12712

Liu ZJ, Sun YJ, Rose J, Chung YJ, Hsiao CD, Chang WR, Kuo I, Perozich J, Lindahl R, Hempel J (1997) The first structure of an aldehyde dehydrogenase reveals novel interactions between NAD^+ and the Rossmann fold. Nat Struct Biol 4:317–326

Lo HF, Chen YJ (2010) Gene cloning and biochemical characterization of a $NAD(P)^+$-dependent aldehyde dehydrogenase from *Bacillus licheniformis*. Mol Biotechnol 46:157–167

Loveridge EJ, Rodriguez RJ, Swanwick RS, Allemann RK (2009) Effect of dimerization on the stability and catalytic activity of dihydrofolate reductase from the hyperthermophile *Thermotoga maritima*. Biochemistry 48:5822–5933

Lunn FA, MacLeod TJ, Bearne SL (2008) Mutational analysis of conserved glycine residues 142, 143 and 146 reveals Gly(142) is critical for tetramerization of CTP synthase from *Escherichia coli*. Biochem J 412:113–121

Mann CJ, Weiner H (1999) Differences in the roles of conserved glutamic acid residues in the active site of human class 3 and class 2 aldehyde dehydrogenases. Protein Sci 8:1922–1929

Mansfeld J, Ulbrich-Hofmann R (2007) The stability of engineered thermostable neutral proteases from *Bacillus stearothermophilus* in organic solvents and detergents. Biotechnol Bioeng 97:672–679

Marchal S, Cobessi D, Rahuel-Clermont S, Téte-Favier F, Aubry A, Branlant G (2001) Chemical mechanism and substrate binding sites of NADP-dependent aldehyde dehydrogenase from *Streptococcus mutans*. Chem Biol Interact 130–132:15–28

Ming LJ, Epperson DJ (2002) Metal binding and structure-activity relationship of the metalloantibiotic peptide bacitracin. J Inorg Biochem 91:48–58

Monera OD, Kay CM, Hodges RS (1994) Protein denaturation with guanidine hydrochloride or urea provides a different estimate of stability depending on the contributions of electrostatic interactions. Protein Sci 3:1984–1991

Moore BM, Flurkey WH (1990) Sodium dodecyl sulfate activation of a plant polyphenoloxidase: effect of sodium dodecyl sulfate on enzymatic and physical characteristics of purified broad bean polyphenoloxidase. J Biol Chem 265:4982–4988

Moore SA, Baker HM, Blythe TJ, Kitson KE, Kitson TM, Baker EN (1998) Sheep liver cytosolic aldehyde dehydrogenase: the structure reveals the basis for the retinal specificity of class 1 aldehyde dehydrogenases. Structure 6:1541–1551

Mouw KW, Steiner AM, Ghirlando R, Li NS, Rowland SJ, Boocock MR, Stark WM, Piccirilli JA, Rice PA (2010) Sin resolvase catalytic activity and oligomerization state are tightly coupled. J Mol Biol 404:16–33

Murphy T, Roy I, Harrop A, Dixon K, Keshavarz T (2007) Effect of oligosaccharide elicitors on bacitracin a production and evidence of transcriptional level control. J Biotechnol 131:397–403

Nakagawa Y, Saburi W, Takada M, Hatada Y, Horikoshi K (2008) Gene cloning and enzymatic characteristics of a novel γ-cyclodextrin-specific cyclodextrinase from alkalophilic *Bacillus clarkii* 7364. Biochim Biophys Acta 1784:2004–2011

Nandi PK, Robinson DR (1984) Effects of urea and guanidine hydrochloride on peptide and nonpolar groups. Biochemistry 23:6661–6668

Ni L, Sheikh S, Weiner H (1997) Involvement of glutamate 399 and lysine 192 in the mechanism of human liver mitochondrial aldehyde dehydrogenase. J Biol Chem 272:18823–18826

Ni L, Zhou J, Hurley TD, Weiner H (1999) Human liver mitochondrial aldehyde dehydrogenase: three-dimensional structure and the restoration of solubility and activity of chimeric forms. Protein Sci 8:2784–2790

Niederreither K, Vermot J, Messaddeq N, Schuhbaur B, Chambon P, Dellé P (2001) Embryonic retinoic acid synthesis is essential for heart morphogenesis in the mouse. Development 128:1019–1031

Pace CN (1990) Measuring and increasing protein stability. Trends Biotechnol 8:93–98

Parés X, Farrés J, Kedishvili N, Duester G (2008) Medium- and short-chain dehydrogenase/reductase gene and protein families: medium-chain and short-chain dehydrogenases/reductases in retinoid metabolism. Cell Mol Life Sci 65:3936–3949

Parsot C, Mekalanos JJ (1991) Expression of the *Vibrio cholerae* gene encoding aldehyde dehydrogenase is under control of ToxR, the cholera toxin transcription activator. J Bacteriol 173:2842–2851

Perez-Miller SJ, Hurley TD (2003) Coenzyme isomerization is integral to catalysis in aldehyde dehydrogenase. Biochemistry 42:7100–7109

Perozich J, Nicholas H, Wang BC, Lindahl R, Hempel J (1999) Relationship within the aldehyde dehydrogenase extended family. Protein Sci 8:137–146

Persson B, Kallberg Y, Bray JE, Bruford E, Dellaporta SL, Favia AD, Duarte RG, Jörnvall H, Kavanagh KL, Kedishvili N, Kisieia M, Maser E, Mindnich R, Orchard S, Penning TM, Thomton JM, Adamski J, Oppermann U (2009) The SDR (short-chain dehydrogenase/reductase and related enzymes) nomenclature initiative. Chem Biol Interact 178:94–98

Plaza del Pino IM, Ibarra-Molero B, Sachez-Ruiz JM (2000) Lower kinetic limit to protein thermal stability: a proposal regarding protein stability in vivo and its relation with misfolding diseases. Proteins 40:58–70

Priefert H, Kruger N, Jendrossek D, Schmidt B, Steinbuchel A (1992) Identification and molecular characterization of the gene coding for acetaldehyde dehydrogenase II (*acoD*) of *Alcaligenes eutrophus*. J Bacteriol 174:899–907

Rachadech W, Navacharoen A, Ruangsit W, Pongtharangkul T, Vangnai AS (2010) An organic solvent-, detergent-, and thermostable alkaline protease from mesophilic, organic solvent-tolerant *Bacillus licheniformis* 3C5. Mikrobiologiia 79:630–638

Rahman RN, Geok LP, Basri M, Salleh AB (2005) Physical factors affecting the production of organic solvent-tolerant protease by *Pseudomonas aeruginosa* strain K. Bioresour Technol 96:429–436

Reynolds JA, Tanford C (1970) Binding of dodecyl sulfate to proteins at high binding ratios: possible implications for the state of proteins in biological membranes. Proc Natl Acad Sci USA 66:1002–1007

Rodríguez-Zavala JS, Ortíz-Cruz MA, Moreno-Sáchez R (2006) Characterization of an aldehyde dehydrogenase from *Euglena gracilis*. J Eukaryot Microbiol 53:36–42

Royer CA (2006) Probing protein folding and conformational transitions with fluorescence. Chem Rev 106:1769–1784

Royer CA, Mann CJ, Matthews CR (1993) Resolution of the fluorescence equilibrium unfolding profile of trp aporepressor using single tryptophan mutants. Protein Sci 2:1844–1852

Schallmey M, Singh A, Ward OP (2004) Developments in the use of *Bacillus* species for industrial production. Can J Microbiol 50:1–17

Schellman JA (2002) Fifty years of solvent denaturation. Biophys Chem 96:91–101

Schuck P (2000) Size-distribution analysis of macromolecules by sedimentation velocity ultracentrifugation and Lamm equation modeling. Biophys J 78:1606–1619

Shafiei M, Ziaee AA, Amoozegar MA (2011) Purification and characterization of an organic-solvent-tolerant halophilic α-amylase from the moderately halophilic *Nesterenkonia* sp. strain F. J Ind Microbiol Biotechnol 38:275–281

Sheikh S, Ni L, Hurley TD, Weiner H (1997) The potential roles of the conserved amino acids in human liver mitochondrial aldehyde dehydrogenase. J Biol Chem 272:18817–18822

Shi Y, Liu JH, Zhang HJ, Ding Y (2008) Equilibrium unfolding mechanism of chicken muscle triose phosphate isomerase. Protein Pept Lett 15:365–370

Sidhu RS, Blair AH (1975) Human liver aldehyde dehydrogenase: esterase activity. J Biol Chem 250:7894–7898

Smith CA (1988) Estimation of sedimentation coefficients and frictional ratios of globular proteins. Biochem Educ 16:104–106

Sophos NA, Vasiliou V (2003) Aldehyde dehydrogenase gene superfamily: the 2002 update. Chem Biol Interact 143–144:5–22

Sripo T, Phongdara A, Wanapu C, Caplan AB (2002) A novel transformation of polychlorinated biphenyls by *Rhodococcus* sp. strain RHA1. Appl Environ Microbiol 62:171–179

Steinmetz CG, Xie P, Weiner H, Hurley TD (1997) Structure of mitochondrial aldehyde dehydrogenase: the genetic component of ethanol aversion. Structure 5:701–711

Tang XY, Pan Y, Li S, He BF (2008) Screening and isolation of an organic solvent-tolerant bacterium for high-yield production of organic solvent-stable protease. Bioresour Technol 99(15): 7388–7392

Vallari RC, Pietruszko R (1984) Interaction of Mg^{2+} with human liver aldehyde dehydrogenase: mechanism and site of interaction. J Biol Chem 259:4927–4933

Vasiliou V, Nebert DW (2005) Analysis and update of the human aldehyde dehydrogenase (ALDH) gene family. Hum Genomics 2:138–143

Vasiliou V, Weiner H, Mareslos M, Nebert DW (1995) Aldehyde dehydrogenase genes: classification based on evolution, structure and regulation. Eur J Drug Metab Pharmacokinet 20:53–64

Vasiliou V, Pappa A, Petersen D (2000) Role of aldehyde dehydrogenase in endogenous and xenobiotic metabolism. Chem Biol Interact 129:1–19

Vecchio PD, Granziano G, Granata V, Barone G, Mandrich L, Rossi M, Manco G (2002) Denaturing action of urea and guanidine hydrochloride towards two thermophilic esterases. Biochem J 367:857–863

Veith B, Herzberg C, Steckel S, Feesche J, Maurer KH, Ehrenreich P, Baeumer S, Henne A, Liesegang H, Merkl R, Ehrenreich A, Gottschalk G (2004) The complete genome sequence of *Bacillus licheniformis* DSM13, an organism with great industrial potential. J Mol Microbiol Biotechnol 7:204–211

Vogl T, Jatzke C, Hinz HJ, Benz J, Huber R (1997) Thermodynamic stability of annexin V E17G: equilibrium parameters from an irreversible unfolding reaction. Biochemistry 36:1657–1668

Wang X, Weiner H (1995) Involvement of cysteine 289 in the catalytic activity of an $NADP^+$-specific fatty aldehyde dehydrogenase from *Vibrio harveyi*. Biochemistry 34:237–243

Wang ZF, Huang MQ, Zou XM, Zhou HM (1995) Unfolding, conformational change of active sites and inactivation of creatine kinase in SDS solutions. Biochim Biophys Acta 1251:109–114

Weretilnyk EA, Hanson AD (1990) Molecular cloning of a plant betainealdehyde dehydrogenase, an enzyme implicated in adaptation to salinity and drought. Proc Natl Acad Sci USA 87:2745–2749

Yoshida A, Rzhetsky A, Hsu LC, Chang C (1998) Human aldehyde dehydrogenase gene family. Eur J Biochem 251:549–557

Yuan Y, Knaggs MH, Poole LB, Fetrow JS, Salsbury FR Jr (2010) Conformational and oligomeric effects on the cysteine pK(a) of tryparedoxin peroxidase. J Biomol Struct Dyn 28:51–70

Zamorano LS, Vilarmau SB, Arellano JB, Zhadan GG, Guadrado NH, Bursakov SA, Roig MG, Shnyrov VL (2009) Thermal stability of peroxidase from *Chamaerops excelsa* palm tree at pH 3. Int J Biol Macromol 44:326–332

Zheng CF, Wang TTY, Weiner H (1993) Cloning and expression of the full-length cDNAs encoding human liver class 1 and class 2 aldehyde dehydrogenases. Alcohol Clin Exp Res 17:828–831

Zuo R (2007) Biofilms: strategies for metal corrosion inhibition employing microorganisms. Appl Microbiol Biotechnol 76(6):1245–1253